From Droplets to Nanowires: Dynamics of Vapor-Liquid-Solid Growth

K. W. Schwarz and J. Tersoff

IBM Research Division, T. J. Watson Research Center, Yorktown Heights, New York 10598, USA

(Received 18 January 2009; published 20 May 2009)

Starting with a liquid eutectic droplet on a surface, we calculate its dynamical evolution into an epitaxial nanowire via the vapor-liquid-solid growth process. Our continuum approach incorporates kinetic effects and crystalline anisotropy in a natural way. Some realistic features appear automatically even for an isotropic solid, e.g., the tapered wire base. Crystal anisotropy leads to a richer variety of morphologies. For example, sixfold anisotropy leads to a wire shape having broken symmetry and an intriguing resemblance to the ⟨110⟩-oriented Si wires seen in Au-catalyzed growth on Si (111), while higher symmetry leads to a shape more like ⟨111⟩ Si wires.

DOI: 10.1103/PhysRevLett.102.206101 PACS numbers: 81.15.Lm, 61.46.Km, 81.07.Vb

In the last decade there has been an explosion of work on the growth of semiconductor nanowires. Most of this work uses the vapor-liquid-solid (VLS) process, in which typically a liquid eutectic droplet catalyzes capture of material from the vapor and incorporation into the solid [1]. The basic VLS mechanism has been understood for decades [1,2], but more recent work has revealed a rich and often puzzling phenomenology. To address this, and to achieve the control required for technology, will require a far more complete understanding. To date there have been useful discussions and analyses, especially for steady-state growth within isotropic models [2–5], but no general method for calculating the dynamical evolution from a droplet into a wire has been reported to our knowledge [6].

Here we present a continuum model for nanowire VLS growth. We apply the model to study how growth begins and evolves toward steady-state wire growth. More complex situations such as catalyst coarsening and interrupted growth [7] are easily handled, as we show. Most importantly, we can study how crystal anisotropy affects the wire morphology and growth direction. For example, Au-catalyzed Si nanowires are most often seen growing in the ⟨111⟩ direction, but ⟨110⟩ and ⟨112⟩ wires are also observed. An isotropic model in two dimensions gives a morphology qualitatively like ⟨111⟩ Si wires. A 12-fold anisotropy increases the similarity. But a sixfold anisotropy leads to a shape with broken symmetry, growing at an angle to the substrate. This shape is very different from ⟨111⟩ wires, but bears a striking resemblance to the wires that grow in the ⟨110⟩ direction. Our growth simulations show not only the final shape but also the entire dynamical evolution, revealing the process by which the symmetry is broken.

Our system consists of a liquid eutectic on a solid surface (e.g., AuSi on Si), as in Fig. 1(a). The liquid can move along the solid surface in response to capillary forces. At the same time, the solid can gain or lose material to the liquid in response to differences in the chemical potentials, which include contributions from capillary forces [8]. Therefore we first address the forces (which may be unbalanced), then calculate the chemical potential including these forces, and finally use these as input to kinetic models of the evolution.

An important aspect of our approach is that even when there is a "sharp" corner, it is actually smooth at some length scale. The solid surface has a minimum radius of curvature, as described below and illustrated in Fig. 1. Thus the forces on the trijunction can always be separated into components normal and tangential to the solid, as for a liquid on a planar solid. Motion of the trijunction along the solid surface is driven by the tangential component, with force per unit length

$$f_c = \gamma_{vs} - \gamma_{ls} - \gamma_{vl}\cos\theta_c \tag{1}$$

with positive force meaning outward from the liquid. Here γ_{vs}, γ_{ls}, and γ_{vl} are the vapor-solid, liquid-solid, and vapor-liquid interface energies per unit area, and θ_c is the contact angle [measured from the local tangent, as in Fig. 1(b)].

In general, this force can be used as input for any desired model of the liquid dynamics. However, in VLS the response of the liquid is fast compared with the growth rate of the solid. Therefore the droplet stays close to mechanical equilibrium: $f_c = 0$, and the liquid-vapor interface has constant mean curvature. These conditions, together with

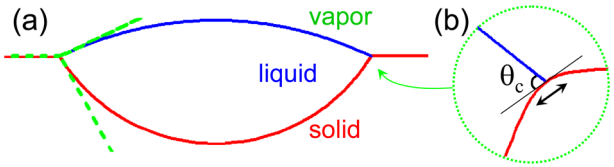

FIG. 1 (color online). (a) Equilibrium morphology of the liquid catalyst on the solid substrate, for parameters in text. Dashed lines show classic equilibrium angles, oriented to be tangent to the droplet at the trijunction, illustrating that these angles are captured correctly by the simulation. (b) Expanded view of trijunction, showing that the solid surface is locally smooth. Double arrow indicates smoothing of corner by w_c. θ_c is contact angle measured from local tangent.

the droplet volume, determine the trijunction position and contact angle as the shape of the solid evolves.

In addition to the tangential force f_c at the trijunction, there is also a force normal to the surface. This force does not contribute to motion of the liquid, but it enters the chemical potential and thus plays a central role in controlling the growth of the solid. The normal force on the solid is

$$p = \gamma_{vl}\kappa_l\Theta_l - \gamma_{vl}\sin\theta_c\delta_c. \quad (2)$$

The Gibbs term ($\gamma_{vl}\kappa_l$) represents the internal pressure of the liquid, where κ_l is the trace of the curvature tensor of the vapor-liquid interface (which is constant over the interface). There is no pressure outside the droplet, as indicated by the step function Θ_l which equals 1 at the liquid-solid interface and 0 at the vapor-solid interface. The second term is the liquid surface tension pulling on the solid. This gives a δ-function distribution of pressure applied at the trijunction. To avoid singularities, we smooth the discontinuous step function Θ_l over a width w_c. (This may be viewed as roughly representing the finite thickness of the liquid-vapor interface, or as merely a mathematical regularization of the discontinuity at the trijunction.) We take the smoothed δ function to be $\delta_c = |\nabla_s\Theta_l|$, where ∇_s is the gradient along the solid surface.

Including the normal force explicitly, the chemical potential μ_s at any point on the surface of the solid can be written [9,10]

$$\mu_s = \Omega_s\left[\kappa\gamma + \boldsymbol{\kappa}\cdot\frac{\partial^2\gamma}{\partial\hat{n}^2} + p + C(\boldsymbol{\kappa})\right]. \quad (3)$$

Generalizing the Gibbs term $\kappa\gamma$ to anisotropic γ adds the second term: the scalar contraction of the curvature tensor $\boldsymbol{\kappa} = -\nabla_s\hat{n}$ and the second-derivative tensor $\partial^2\gamma/\partial\hat{n}^2$, $\hat{n}$ being the unit normal vector defining surface orientation. The interface energy changes across the trijunction, with a step function $\gamma = \gamma_{ls}\Theta_l + \gamma_{vs}(1-\Theta_l)$. Note that γ_{ls} and γ_{vs} are orientation dependent, so $\gamma = \gamma(\hat{n})$. Ω_s is the atomic volume, and $C(\kappa)$ is a standard regularization term that limits the sharpness of edges on faceted surfaces [9].

We also need the chemical potential μ_l in the liquid. This is treated in detail in Ref. [5]. For the present study we take a simplified illustrative model,

$$\mu_l = \beta(c_l - c_0) + \Omega_l\gamma_{vl}\kappa_l. \quad (4)$$

For liquid composition c_l, the first term represents the supersaturation with respect to the equilibrium liquidus concentration, taken here as $c_0 = 0.2$. Thus β reflects the derivative of μ or second derivative of free energy with respect to composition. The second term is the Gibbs-Thomson effect of surface tension, with Ω_l being the specific volume in the liquid.

Given the chemical potentials, we can now address the growth kinetics. In VLS growth, the liquid captures material from the vapor and deposits it onto the solid. Ideally the number N_{cat} of catalyst atoms remains fixed. But the number N_g of atoms of the growth material (e.g., Si for AuSi-Si) can evolve, along with their chemical potential μ_l in the liquid. If the liquid is close to equilibrium with the vapor, then μ_l is a constant controlled experimentally via the vapor, as for Si growth from $SiCl_4 + H_2$ [2]. More generally, if material is added at a rate Φ_g (atoms/time), the amount of solute N_g evolves as

$$\frac{dN_g}{dt} = \Phi_g - \Omega_s^{-1}\int v_s\, dA, \quad (5)$$

where dA is an area element of the interface, and v_s is its velocity. Integrating Eq. (5) gives N_g and hence the evolving composition $c_l = N_g/(N_{\text{cat}} + N_g)$. For our simulations, we use a model appropriate for Au-catalyzed Si growth from disilane [11], where $\Phi_g = r_{vl}A_{vl}/\Omega_s$. Here A_{vl} is the vapor-liquid interface area, and r_{vl} is a rate constant which depends on temperature and on the partial pressure of the source gas in the vapor, but not on μ_l.

For the liquid-solid kinetics, we use the simplest kinetic model that seems consistent with experiment, assuming that liquid diffusion is fast compared with the time scale of growth, and that attachment and diffusion on the sidewall are negligible. Then crystal growth is controlled by attachment at the liquid-solid interface:

$$v_s = \alpha_{ls}(\mu_l - \mu_s), \quad (6)$$

where v_s is the local growth velocity of the solid. The kinetic rate coefficient α_{ls} is taken as nonzero only at the liquid-solid interface, where it is isotropic and independent of position. [Kinetic anisotropy can be easily included in α in Eq. (6).]

In our numerical implementation, for simplicity we restrict ourselves to two dimensions (2D). We track the solid surface using discrete points with variable spacing and spline interpolation; so it is straightforward to ensure that the point spacing is everywhere much smaller than the local radius of curvature (e.g., much smaller than w_c at the trijunction in Fig. 1). To reduce the number of parameters, we focus on the limit of small w_c and large β, decreasing w_c and increasing β until the growth behavior converges. In this large-β limit, c_0 and Ω_l become irrelevant: the liquid is merely a conduit for material, and μ_l adjusts to ensure that the growth rate exactly balances the incoming flux Φ_g at all times.

We begin with the static equilibrium, $\Phi_g = 0$, of an isotropic solid. We take $\Omega_s\gamma_{vs} = 0.16$ eV nm, $\Omega_s\gamma_{ls} = 0.07$ eV nm, $\Omega_s\gamma_{vl} = 0.14$ eV nm, and 2D liquid "volume" of 6250 nm^2 on a semi-infinite solid. These four numbers set the energy scale, the length scale, and the two independent angles of the equilibrium trijunction [12]. Integrating Eq. (6) to equilibrium [i.e., allowing nonzero α everywhere instead of just at the liquid-solid (LS) interface in Eq. (6)], we obtain the geometry shown in Fig. 1.

On the scale of Fig. 1(a), the shape appears indistinguishable from the classic "oil drop on water" shape with

angles given by balancing all capillary forces [12]. The classic angles calculated from the surface energies are shown as dashed lines, and they correspond well to the tangents at the trijunction.

A closer view of the trijunction is shown in Fig. 1(b). The surface is actually smooth on a scale set by w_c or $C(\kappa)$; here we take $w_c = 0.4$ nm, and we omit $C(\kappa)$ for the isotropic case. The microscopic contact angle in Fig. 1(b) is consistent with Young's equation (force balance tangent to the surface) [12].

The ratio r_{vl}/α_{ls} between vapor-liquid and liquid-solid rate constants determines whether we are in the regime of slow growth (liquid near equilibrium with solid) or fast growth (large liquid supersaturation). Since α_{ls} and r_{vl} are both thermally activated, but with very different activation energies, r_{vl}/α_{ls} can span a huge range depending on the system and the growth temperature.

Beginning from equilibrium, we grow at different rates Φ_g. The result are shown in Fig. 2. For relatively slow growth ($r_{vl}/\alpha_{ls} = 0.5$ meV) the apparent angles at the steady-state trijunction are close to their equilibrium values, as shown in Fig. 2(b). Increasing the growth rate or decreasing α_{ls} by a factor of 2000 flattens the growth front dramatically, as shown in Fig. 2(c).

Often nanowire growth is not steady state. A good example is the tapering of Au-catalyzed Si nanowires due to diffusion of Au from one wire to another [7]. Our model can easily accommodate such processes. The Au chemical potential is well understood in principle [5], so one can calculate the diffusion between wires, given some model for the diffusion and attachment kinetics. Here we illustrate the effect of such coarsening on wire morphology by simply letting the amount of catalyst increase or decrease at a constant rate $dN_{\rm cat}/dt = \Phi_{\rm cat}$.

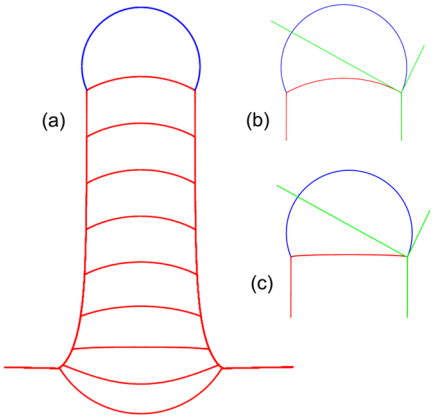

FIG. 2 (color online). (a) Evolution from equilibrium droplet to steady-state nanowire growth, for relatively slow growth. Successive lines from bottom to top show outline of crystal at equal time increments during growth. Circular arc at top is liquid at final time. (b) Region around growth front, for final geometry of (a). Straight lines show classic equilibrium angles (i.e., calculated from the γ values), oriented to be tangent to droplet at trijunction. Trijunction angles during slow growth are found to be close to the equilibrium values here. (c) Same as (b), for relatively fast growth, showing change in shape of growth front and angles due to kinetics.

Growing at a constant rate, we obtain the tapered morphologies shown in Figs. 3(a) and 3(b). The degree of taper simply reflects the ratio $\Phi_{\rm cat}/\Phi_g$. If we interrupt the growth, so that $\Phi_g = 0$ for some period while $\Phi_{\rm cat}$ remains unchanged, we find the morphologies shown in Figs. 3(c) and 3(d). This is quite similar to the morphologies seen experimentally when growth is interrupted [7].

Most semiconductors are strongly faceted. Our approach makes it straightforward to include highly anisotropic surface energies. Thus we can study by direct simulation how anisotropy affects the growth dynamics and the final wire morphology. Here we use a minimal model [9] for the surface energy anisotropy

$$\gamma \rightarrow \gamma(1 - \epsilon_n \cos n\theta) \tag{7}$$

where for simplicity we multiply both γ_{vs} and γ_{ls} by the same dimensionless anisotropy factor $(1 - \epsilon_n \cos n\theta)$. The angle θ is the local surface orientation in our 2D model; the 3D generalization is given in Ref. [9]. This model does not give strictly planar facets, but for large enough ϵ is gives an equilibrium crystal shape with n nearly flat faces meeting at sharp corners.

We first consider $n = 12$ and $\epsilon_{12} = 0.02$, equilibrating a droplet of liquid and then growing at the same rate as in Fig. 2(a). The result is shown in Fig. 4(a). The substrate orientation is $\theta = 0$, a minimum-energy orientation. The equilibrium crystal shape is reflected in the initial LS interface before growth. In many ways, the growth appears similar to the isotropic result of Fig. 2. There are also intriguing differences. In steady-state growth, the LS interface is quite flat and normal to the sidewall. The wire base is a faceted pedestal as seen in some experiments, rather than smoothly tapered as in Fig. 2.

The behavior changes dramatically for $n = 6$. The LS interface takes a stable orientation as before. However, the orientation normal to this is not stable; so if the sidewall

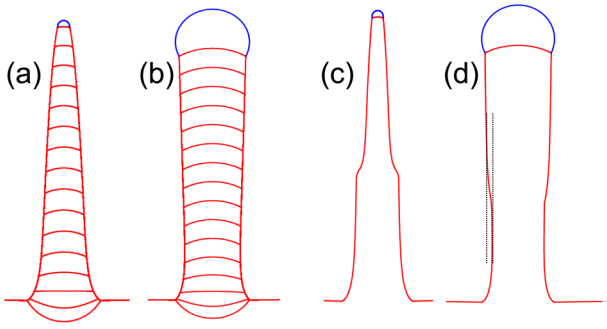

FIG. 3 (color online). Catalyst coarsening with and without interruption. Steady loss (a) or gain (b) of catalyst during growth leads to smoothly tapering wire. Interrupting the growth halfway through, while catalyst loss (c) or gain (d) continues, leads to an abrupt change in width [highlighted by dotted lines in (d)]. Similar behavior has been seen in experiment [7].

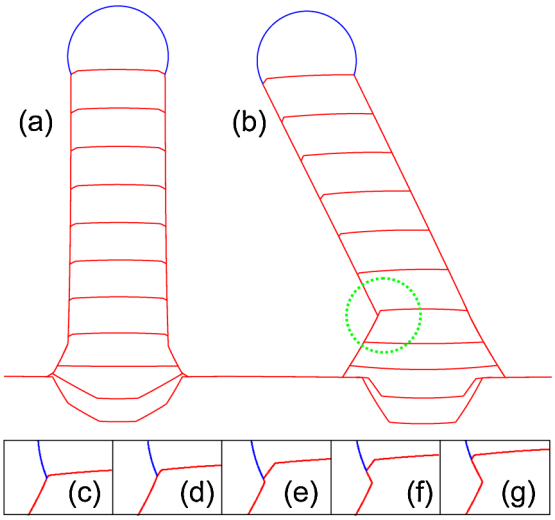

FIG. 4 (color online). (a) Growth of wire with 12-fold anisotropy described in text. Lines show outline of solid at successive times. The lowest line is initial equilibrium structure. Circular arc at top is liquid-vapor interface at final time shown. (b) Same for sixfold anisotropy described in text. (c)–(g) Time sequence for region indicated by dotted circle in (b), at much shorter time intervals, showing how the droplet (d) unpins from the corner and slides down the sidewall, and (e) introduces a new facet which in (f),(g) becomes the new sidewall, thereby breaking the symmetry and initiating the steady-state growth morphology.

takes a low-energy orientation, it cannot meet the LS interface at a right angle. Instead the wire grows at an angle, as seen in Fig. 4(b) for $\epsilon_6 = 0.10$. It is intriguing to note that the morphology for 12-fold anisotropy resembles that of Au-catalyzed Si nanowires growing in the $\langle 111 \rangle$ direction on a (111) substrate, while the sixfold case of Fig. 4(b) resembles $\langle 110 \rangle$ wires [13].

Even more intriguing than the steady-state growth is how the wire reaches an asymmetric geometry from a symmetric beginning. Figure 4(b) includes the outline of the solid at successive times. Initially, the LS interface evolves to fill in the initial depression and build a tapering mound, much as in the isotropic and 12-fold cases. As a result, the droplet is squeezed onto an increasingly narrow pedestal.

Eventually the pedestal becomes too narrow, and the situation becomes unstable. At that point, as shown in Figs. 4(c)–4(g), the droplet unpins from a corner (c),(d), and slides (c)–(e) far enough down the sidewall (e) to relieve the force on both trijunctions. This breaks the reflection symmetry and (e) initiates growth (f),(g) of a new facet.

Before performing these simulations, we expected that the trijunction would advance monotonically forward, and that the final sidewalls were simply a trace of the trijunction trajectories [3]. Instead, the evolution is at once more complex and easier to understand. It was unanticipated because the final wire geometry hides the complexity of the dynamic trajectory. *In situ* microscopy during growth shows that such jumps are a common feature in nanowire growth in some conditions [14].

In conclusion, our kinetic model makes it possible to directly simulate VLS growth, including growth of a nanowire from a catalyst droplet. Our initial studies already reveal unexpected details of the growth dynamics, such as how new facets are introduced during the approach to steady-state growth. We expect that in the future this approach will make possible a more direct coupling of theory and experiment, providing further insight into nanowire growth.

We gratefully acknowledge helpful discussions with W. C. Carter, F. M. Ross, V. Schmidt, V. B. Shenoy, B. J. Spencer, and P. W. Voorhees.

[1] R. S. Wagner and W. C. Ellis, Appl. Phys. Lett. **4**, 89 (1964); R. S. Wagner, in *Whisker Technology*, edited by A. P. Levitt (Wiley: Interscience, NY, 1970), p. 47.
[2] E. I. Givargizov, J. Cryst. Growth **31**, 20 (1975).
[3] F. M. Ross, J. Tersoff, and M. C. Reuter, Phys. Rev. Lett. **95**, 146104 (2005).
[4] V. Schmidt, S. Senz, and U. Gösele, Phys. Rev. B **75**, 045335 (2007).
[5] S. M. Roper, S. H. Davis, S. A. Norris, A. A. Golovin, P. W. Voorhees, and M. Weiss, J. Appl. Phys. **102**, 034304 (2007).
[6] A pioneering calculation of the evolution was reported by V. Schmidt, S. Senz, and U. Gösele, Appl. Phys. A **80**, 445 (2005). That model considered an isotropic solid-vapor interface but strictly planar solid-liquid interface, and assumed that forces balance tangent to the solid-liquid interface, and that the trijunction never moves off the sharp corner. We find that these assumptions are not valid for the more interesting case where the solid-vapor interface is also facetted, highlighting the need for a more general and rigorous approach.
[7] J. B. Hannon, S. Kodambaka, F. M. Ross, and R. M. Tromp, Nature (London) **440**, 69 (2006).
[8] The sometimes confusing connection between mechanical and chemical terms at interfaces is discussed by P. Nozieres, in *Solids Far from Equilibrium*, edited by C. Godreche (Cambridge University Press, Cambridge, 1992), Chap. 1; and by C. Caroli and C. Misbah, J. Phys. I (France) **7**, 1259 (1997).
[9] A. Mastroberardino and B. J. Spencer (to be published); B. J. Spencer, Phys. Rev. E **69**, 011603 (2004).
[10] The forces cause elastic distortions of the solid. These make a contribution to μ_s that scales inversely with elastic modulus, and can be neglected here.
[11] S. Kodambaka, J. Tersoff, M. C. Reuter, and F. M. Ross, Phys. Rev. Lett. **96**, 096105 (2006).
[12] See, e.g., E. Saiz, A. P. Tomsia, and R. M. Cannon, Acta Mater. **46**, 2349 (1998), and references therein.
[13] S. Kodambaka, J. B. Hannon, R. M. Tromp, and F. M. Ross, Nano Lett. **6**, 1292 (2006).
[14] F. M. Ross and S. Kodambaka (private communication).